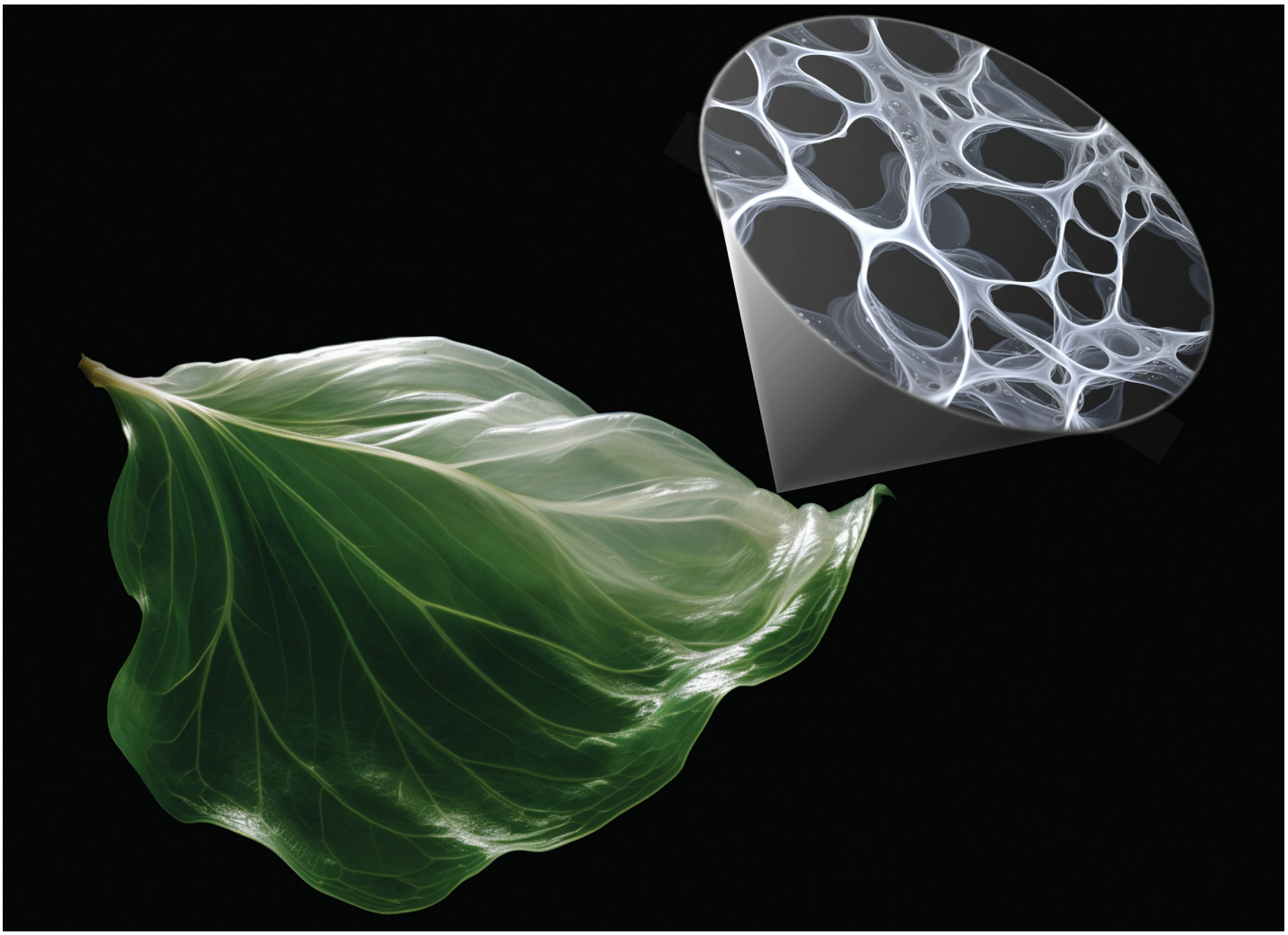

Showcasing research from Professor Piero Baglioni's laboratory, School of Chemistry, University of Florence and CSGI, Florence, Italy.

New horizons on advanced nanoscale materials for Cultural Heritage conservation

Ultra-adaptive and adhesive hydrogels, obtained at the Centre for Colloid and Surface Science (CSGI) from green and sustainable materials, feature a hierarchical porosity and a high tortuosity at the nanoscale. This grants enhanced sorption and cleaning abilities, of specific interest in applications related to the restoration of artworks and conservation of Cultural Heritage in general.These materials can impact on fields even beyond art preservation, like drug delivery, detergency, food industry, cosmetics and tissue engineering.

As featured in:

See Piero Baglioni *et al.*, *Nanoscale Horiz.*, 2024, **9**, 566.

ROYAL SOCIETY OF CHEMISTRY

rsc.li/nanoscale-horizons

Registered charity number: 207890

Nanoscale Horizons

ROYAL SOCIETY OF CHEMISTRY

COMMUNICATION

View Article Online
View Journal | View Issue

Cite this: *Nanoscale Horiz.*, 2024, 9, 566

Received 30th August 2023,
Accepted 2nd January 2024

DOI: 10.1039/d3nh00383c

rsc.li/nanoscale-horizons

New horizons on advanced nanoscale materials for Cultural Heritage conservation

Rosangela Mastrangelo, David Chelazzi and Piero Baglioni *

Nanomaterials have permeated numerous scientific and technological fields, and have gained growing importance over the past decades also in the preservation of Cultural Heritage. After a critical overview of the main nanomaterials adopted in art preservation, we provide new insights into some highly relevant gels, which constitute valuable tools to selectively remove dirt or other unwanted layers from the surface of works of art. In particular, the recent "twin-chain" gels, obtained by phase separation of two different PVAs and freeze-thawing, were considered as the most performing gel systems for the cleaning of Cultural Heritage. Three factors are crucial in determining the final gel properties, *i.e.*, pore size, pore connectivity, and surface roughness, which belong to the micro/nanodomain. The pore size is affected by the molecular weight of the phase-separating PVA polymer, while pore connectivity and tortuosity likely depend on interconnections formed during gelation. Tortuosity greatly impacts on cleaning capability, as the removal of matter at the gel–target interface increases with the uploaded fluid's residence time at the interface (higher tortuosity produces longer residence). The gels' surface roughness, adaptability and stickiness can also be controlled by modulating the porogen amount or adding different polymers to PVA. Finally, PVA can be partially replaced with different biopolymers yielding gels with enhanced sustainability and effective cleaning capability, where the selection of the biopolymer affects the gel porosity and effectiveness. These results shed new light on the effect of micro/nanoscale features on the cleaning performances of "twin-chain" and composite gels, opening new horizons for advanced and "green"/sustainable gel materials that can impact on fields even beyond art preservation, like drug-delivery, detergency, food industry, cosmetics and tissue engineering.

New concepts

Among the systems adopted in Cultural Heritage preservation, gels are highly advantageous since they grant selective removal of unwanted layers from artistic surfaces. However, fundamental insights are needed regarding the effects of the gels' surface and structural features at the micro/nanoscale, on their interaction with target surfaces, and on matter transport in the gels. We shed new light on these aspects considering a recent, innovative class of gels, "twin-chain" polyvinyl alcohol polymer networks (TC-PNs), and monitoring the effect of different PVAs or other polymers on the gels' porosity, surface roughness, and tortuosity. The PVA molecular weight affects pore size in the TC-PN, while tortuosity, generated by connections and structural features at the micro- and nanoscale, favors matter removal by increasing the cleaning fluid's residence time at the gel-target interface. Surface roughness, adaptability and stickiness, crucial factors in cleaning interventions, can be controlled modulating the amount of porogen or adding different polymers to PVA. Finally, PVA can be partially replaced with biopolymers yielding gels with enhanced sustainability. These results open new horizons in the formulation of "green" TC and composite gels, potentially impacting on fields beyond art preservation, like drug-delivery, detergency, food industry, cosmetics and tissue engineering.

Introduction

Almost 65 years after the seminal talk given by Richard Feynman at an American Physical Society meeting, and 50 years after the term "nanotechnology" was coined by Norio Taniguchi at Tokyo Science University, nanomaterials have been adopted in several scientific and technological fields, ranging from bioscience, pharmaceuticals and medicine to energy, textile, food, aerospace, and information industries.[1–4] Nanomaterials have enhanced physico-chemical properties related to their high surface areas, and their applicability in multiple fields is boosted by the possibility of surface functionalization and combination with bulk materials in hybrid systems.[5–10] Over the past decades, these advantageous characteristics have driven the progressive employment of nanoscale systems even in Cultural Heritage (CH) preservation,[11–21] a strong interdisciplinary field where materials science merges with industry, social science and humanities.[22,23] Movable and immovable works of art, along with natural and urban landscapes, are crucial socioeconomic resources, provided that they are preserved against damage caused by environmental and anthropic factors.[24] Even though they involve different ethics, a comparison can be made between medicine and CH preservation,

Department of Chemistry and CSGI, University of Florence, Via della Lastruccia 3, Sesto Fiorentino, FI 50019, Italy. E-mail: baglioni@csgi.unifi.it

to illustrate the importance of remedial and preventive art conservation, and the impact of nanomaterials. As in medicine, diagnostics have been widely developed to gain understanding of the degradation processes that inevitably affect works of art.[25–33] However, prevention and remedial interventions must be specifically designed to conserve and restore the artworks, as much as preventive health care and pharmaceuticals must be devised to cure the patients.[20] Biosystems are regulated by nanoscale structures and processes occurring at the same scale;[34] similarly, works of art degradation typically starts in nano- or mesoscale domains at interfaces and exposed surfaces. Not surprisingly, then, nanomaterials are considered as valuable alternatives to traditional interventions in biomedicine[35] as well as in CH conservation. Even though nanoscale components occur naturally in biological products and food,[36] devising new systems in pharmaceutics and drug delivery requires dedicated research effort in soft matter, colloids, and bioscience.[37,38] Likewise, while numerous types of ancient or classic artifacts include nanostructures produced from practical knowledge and craftmanship over the ages,[39–42] full scientific awareness and tailored design of nanoscale systems in CH conservation only started in the 1980s. Following from the first pioneering studies in this period,[19] nanoscience and colloids have produced a wide range of tools like nanoparticles, gels, microemulsions, coatings, and nanocomposites, which are progressively revolutionizing the conservation practice. However, the field is still open and rich with issues to be solved, owing to the complexity of works of art and their degradation pathways, as well as to the need of high time- and cost-effective tools coping with the preservation of vast collections and extended urban, rural, or archaeological CH assets worldwide. Finally, the imperatives of the Green Deal are urgently calling for the design of materials with enhanced sustainability, reduced ecotoxicological impact, and feasible applicability.[43,44] Sustainability criteria comprise: (i) the use of renewable sources or recycled wastes as raw materials for designing new solutions; (ii) minimizing the amount of raw materials needed; (iii) the use of low-energy processes in the formulation of new materials; (iv) the reduction of waste at the end and throughout the formulation process; (v) the use of raw materials and final products with high green metrics and low ecotoxicological impact, *e.g.*, as indicated by REACh and other regulations.[45–49] These criteria must be included in "safe by design" approaches to the formulation of new materials, and in their evaluation through life cycle assessment.[50,51] Finally, in some cases, the use of materials whose sustainability is not yet fully implemented could be justified if they represent the sole available solution for the timely preservation of irreplaceable CH objects that otherwise would be irreparably lost to degradation.

Altogether, these challenges set new horizons for advanced nanoscale materials that must be useful to multiple fields, from CH preservation to linked sectors like cosmetics, detergency, food industry, tissue engineering, drug-delivery, and others.

Starting with an overview of the main state-of-the-art nanomaterials developed for CH preservation over the past years, this contribution also provides new data on the design and physico-chemical characterization of a highly relevant class of systems, gels, where nano- and mesoscale structural features are central in determining functional properties and efficacy in cleaning artworks, *i.e.*, the removal of soil, aged coatings and adhesives, or even vandalism, which jeopardize canvas paintings, murals, and other iconic types of artifacts. Cleaning is a recurrent issue in restoration, and artworks are typically sensitive to aqueous fluids or organic solvents that, if not properly controlled, can leach or damage original components. Thus, the design of gels as confining networks for the cleaning fluids is essential to achieve selective and effective interventions.[52–55]

New synthetic approaches and gel formulations will be illustrated, along with current challenges, showing how factors like pore interconnectivity and tortuosity in gels affect cleaning capability. Particular attention will be dedicated to new sustainable gelled systems to improve on existing formulations and set new standards in this challenging and exciting field.

Nanoscale materials for Cultural Heritage conservation – an overview

The preservation of iconic fresco paintings from the Renaissance set the ground for the development and assessment of the first nanoscale materials specifically designed for the remedial conservation of Cultural Heritage. Murals are typically polluted by salts, organic contaminants, or aged coatings from past restorations, overall producing the powdering or flaking of painted layers. Therefore, cleaning and consolidation are two recurring tasks in the preservation of these artworks. Namely, the removal of wax contamination from a fresco in Florence (Italy) in the late 1980s, called for the design of an oil-in-water (o/w) microemulsion where dodecane was confined as nanodroplets in nanosized micelles of sodium dodecyl sulphate and 1-pentanol (as the cosurfactant[19]). The large surface area and fast solvent/surfactant exchange dynamics of the micelles, their capability to include wax and transport it in the water phase, and the large aqueous content of the system ($>85\%$ w/w), all made the o/w microemulsion a more efficient tool, and with reduced ecotoxicological impact, than using the same mass of a bulk solvent. Starting from this pioneering study, several o/w nanostructured cleaning fluids have been designed over the past decades, targeting different types of unwanted layers.[52,54,56] Partially water-soluble solvents were adopted, which are partitioned between the continuous aqueous phase and the micelles, enhancing the exchange capability of the fluids with polymer coatings. As a result, layers of synthetic polymers such as acrylate, vinyl, and epoxy, which typically degrade and jeopardize the artifacts' surface, can swell, detach or dewet from the artwork's surface, following the interaction with the fluid. In particular, the presence of solvents for the polymer and highly surface-active surfactants are the key to boost the polymer's dewetting kinetics by mobilizing polymer chains and creating new polymer–fluid and fluid–substrate interfaces.[57–60] This approach is advantageous since it can actually remove the coatings, rather than merely solubilizing and transporting them in the artwork's pores, as can occur with

bulk, non-confined solvents. Water-in-oil (w/o) microemulsions are also being considered for soil removal from highly water-sensitive modern canvas paintings, since a continuous hydrocarbon phase is more inert to the paints' components, while the confined water nanodroplets can remove hydrophilic dirt.[61] Currently, the focus on the design of o/w and w/o microemulsions is on employing "green" solvents and cleavable or degradable surfactants, while maintaining the efficacy of the best-performing fluids.[52,56,62]

Another significant advancement in cleaning formulations came from the design of chemical or physical gel networks to confine the cleaning fluids. Two relevant examples are, respectively, semi-interpenetrated polymer networks (SIPNs) and "twin-chain" polymer networks (TC-PNs). In the first case, a monomer undergoes radical crosslinking in the presence of a linear polymer, which remains entangled in the formed covalent network. The resulting SIPN exhibits the properties of both its parent polymers, like optimal mechanical properties and high hydrophilicity, which are required to handle, apply, and remove gels in cleaning interventions, and to release aqueous fluids at controlled rates without risks for water-sensitive substrates.[11,63–65] Tuning the content of the two components produces SIPNs with different pore size distributions, *i.e.*, more, or less retentive, complying with different cleaning requirements. In the case of TC-PNs, two types of polyvinyl alcohols (PVAs) with different molecular weights and alcohol/acetate ratios are blended in pre-gel solutions. The different molecular weight and hydrophilicity of the PVAs leads to demixing and phase separation in solution, where one of the polymer forms water-swollen micrometric blobs dispersed in the continuous phase of the other PVA.[66] When the solution is freeze-thawed, and then washed, the blobs elongate, partially merge, and release polymers, leaving a spongy, interconnected porous network in the main PVA gel. Part of the second PVA is retained in the pores' walls and makes the network mechanically compliant. These features have made the TC-PNs ideal tools to clean the rough painted surfaces found in modern/contemporary canvas paintings, as demonstrated by the successful cleaning of masterpieces like works by Pablo Picasso, Roy Lichtenstein, and others.[66–69] It must be noticed that, in addition to their micron-sized pores, gel networks also have nanometer-sized porosity and structural elements, including mesh sizes, persistence lengths in swollen chain domains, solid-like inhomogeneities, and crystallites, whose dimensions and extension can be controlled by the synthetic approach. These nanoscale features impact on the mechanical behaviour and retentiveness of the gels, as they participate in the dynamics of the fluids confined in the gels, including the transport of fluids and matter in the gel network, and their exchange at the interface between the gel and the target surface.[64,70] As seen for the nanostructured cleaning fluids, research is currently focusing on the formulation of gels using bio- or natural compounds, which are being progressively adopted to design hydro- (for aqueous fluids) or organogels (able to load organic solvents).[71–77]

Regarding the consolidation of works of art, nanoparticles of alkaline earth hydroxides constitute the first and main example of nanoscale materials designed for the restoration of murals, mortar, and stones.[78–80] Different synthetic approaches, such as top-down and bottom-up routes, have been adopted since the early 2000s to produce particles' dispersions in water or organic solvents. Once applied to the artifacts, the solvent evaporates leaving the nanoparticles adhered to the pores of mural/mortar/stone, where they react with atmospheric CO_2 and turn into a well-adhered and cohered carbonate network that bonds flaking pigments and consolidates surface layers. This approach has optimal physico-chemical compatibility to the original artifacts as opposed to detrimental coatings of polymeric adhesives. As a result, durable consolidation has been achieved on works of art spanning from the European classic ages and Renaissance to Mesoamerican heritage in tropical settings.[11,20] Fundamental studies have also been dedicated to the kinetics of the carbonation process as affected by temperature and relative humidity, using deceleratory or boundary nucleation and growth models.[81,82] Namely, the relative humidity and the nanoparticles' surface area are the key to boost the kinetics, with comparable activation energies to those of high temperature dry solid–gas carbonation processes. These particles can also be used to consolidate silicate stones or earthen materials, as they are able to react with silica and form calcium silicate hydrate (CSH) gel phases that ultimately strengthen the weakened layers.[83] Notably, alkaline earth metal hydroxide nanoparticles proved beneficial also to regulate pH in cellulose- or collagen-based works of art, such as paper, canvas, wood, parchment, and leather.[80,84–86] The selection of dispersion solvents is crucial in this case to avoid damage to fibres, inks, or dyes. Waterlogged wood and shipwrecks like the Vasa and the Mary Rose represent highly challenging cases, where, despite promising results, the homogeneous penetration of the complex 3D wooden matrix by the particles remains an open issue, along with the feasibility of applications on large hulls.[85,87,88]

Finally, nanoscale materials like metal (or metal oxide) particles, nanocarriers, and inorganic–organic hybrids have been explored in the past few years to counteract microorganisms, corrosion, environmental pollutants (as acetic acid), and weathering, or to provide mechanical consolidation. Some examples include silver[89,90] or titanium dioxide nanoparticles,[91,92] and zinc oxide micro- or nanoparticles,[93–95] also embedded in polymer matrices, layered double hydroxides nanocarriers,[96] mesoporous silica nanoparticles,[97] halloysite nanotubes,[98,99] cellulose nanocrystals/fibrils or lignin nanoparticles,[100] cellulose-fibroin colloidal dispersions,[101] and starch nanoparticles.[102] These examples are representative of the potential that nanoscience and colloids have in the formulation of materials for the preservation of CH, with particular emphasis on bio- or biomimetic systems with enhanced properties and reduced ecotoxicity. The promising results obtained so far demonstrate that this is a vibrant research field with a large room for new discoveries and impacts on multiple sectors.

New insights into materials for cleaning works of art

Despite many efforts to refine and enhance the cleaning abilities of gelled systems, there are some crucial aspects that

must be addressed in the current and future research studies to formulate innovative restoration tools. In this contribution, we are providing new experimental data to shed light on three main open aspects in the design of gel formulations: (i) the role of gel network's tortuosity in the cleaning process; (ii) the need for gels able to work on smooth, vertical surfaces; (iii) the incorporation of biobased components into the gel network. In the following sections, we illustrate novel gel formulations tackling these challenges in the cleaning of works of art.

Tailoring porosity, surface roughness, and tortuosity in gels to optimize cleaning capability

The cleaning mechanism occurring at the gel–artwork interface remains largely unexplored. Some intrinsic properties of gels are critical, like porosity, which affects transport properties and surface adhesiveness.

The pores size, morphology and interconnectivity of a gel drastically affect its permeability,[103] the absorption/desorption and retention/release,[104–106] the transport properties, and the matrix tortuosity, *i.e.* the irregularity of the flow/diffusional path. The link between tortuosity in gels and their cleaning capability is one of the fundamental missing pieces towards the rational formulation of optimized cleaning systems, while relevant background on tortuosity exists in the literature regarding membranes[107–110] and porous matrices.[111–114]

Pores connectivity at the micrometer-scale, observed through techniques such as confocal laser scanning microscopy (CLSM), can often be directly related to the connectivity at the nanoscale (see the following paragraphs).[115] The features of PVA-based cryogels at the nanoscale have been investigated through small angle X-ray scattering (SAXS).[66,70,115] These gels are generally characterized by two characteristic dimensions: polymer crystallite radius, 4–6 nm, and a mesh-size, 3–6 nm. The presence of pores in the 50–500 nm size range was also established through scanning electron microscopy imaging.[66,115] Such hierarchical porosity grants enhanced transport properties.

A simplified scheme of the main mechanisms occurring during the cleaning process is shown in Fig. 1. More specifically, a macroporous gel is in contact with a model surface. In Fig. 1, left panel, sub-micron scale details of the gel–substrate interface are shown: a water layer at the interface allows the solubilization of hydrosoluble molecules (in yellow) that diffuse through the interconnected gel pores.

Gels' adhesiveness is another crucial factor influencing cleaning abilities. The adhesiveness of a surface is the result of the interplay between several factors. Specific chemical moieties can affect surface energy and wetting properties,[116–118] and thus promote or limit the interaction with a specific substrate. Surface roughness determines the number of contact points between the gel and the surface. Micron-sized inhomogeneities of the gel surface are ideal to entrap dust or dirt particles (see Fig. 1, right panel). In addition, the surface roughness at the micrometer-scale can be related to the pore morphology, to some extent.

Briefly, the presence of interconnected, micron-sized pores grants the formation of a sponge-like structure, which is

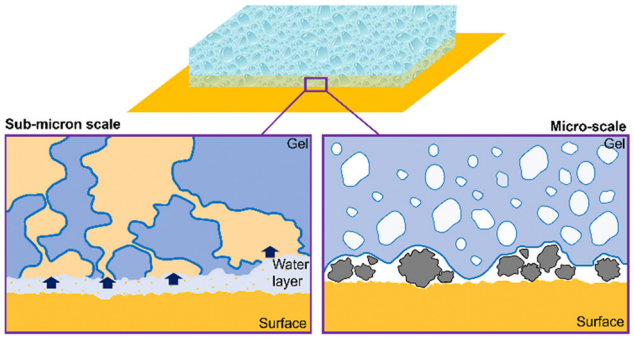

Fig. 1 Simplified scheme of the main processes occurring at the gel–substrate interface during the cleaning process. Left panel: At the sub-micron scale, the detachment and dissolution of the water-soluble components in a thin water layer, which forms at the gel–substrate interface, can be observed. Then, solubilized molecules diffuse through the gel pores. Right panel: At the micro-scale, the entrapment of soil and insoluble particles in the gel nooks can be observed. Higher gel roughness favors the process.

advantageous for the solubilization of hydrosoluble compounds at the interface: in the sponge-like gel, the tortuosity is enhanced, and the residence-time of water at the gel–substrate interface is higher, allowing higher dirt removal.[115] Moreover, sponge-like gels are characterized by a higher surface roughness, which improves adhesivity and dirt-capture at the interface.

It has been recently shown that gels with more pronounced tortuosity exhibit the enhanced removal of hydrosoluble molecules, since longer residence times of the cleaning fluid at the gel–substrate interface allow higher local removal, before the liquid diffuses through the gel matrix[115] (see Fig. 1, left panel). More specifically, it has been found that gels with straight micron-sized pores (such as H-PVA gel (Fig. 2)) are characterized by a lower tortuosity at the nanoscale than sponge-like gels. This implies a link between gels' features at the micro- and nanoscale.

Networks tortuosity can be calculated through fluorescence correlation spectroscopy (FCS) measurements. The apparent tortuosity of the gels can be calculated as the effective relative diffusivity:[115,119,120]

$$D_{sol}/D_{gel} = \tau^2/\varepsilon = {\tau_{app}}^2 \quad (1)$$

where ε is the gels' porosity, and τ^2, the tortuosity factor, is the square of the geometrical tortuosity τ. D_{sol} and D_{gel} represent, respectively, the diffusion coefficient of a free, non-confined dye in aqueous solution and inside the gel.

In principle, macroporous gels can be obtained through different processes, such as solvent casting, freeze drying, gas foaming[121–123] and phase-separation. The latter was recently used to produce sponge-like gels, with interconnected pores.[65,66,115,124] Interconnectivity likely promotes cleaning capability, as dirt is transported through the gel matrix from the gel–artifact interface towards the evaporation front.[66]

While polymers' incompatibility in water already provides the micron-sized domain that act as templates during freezing

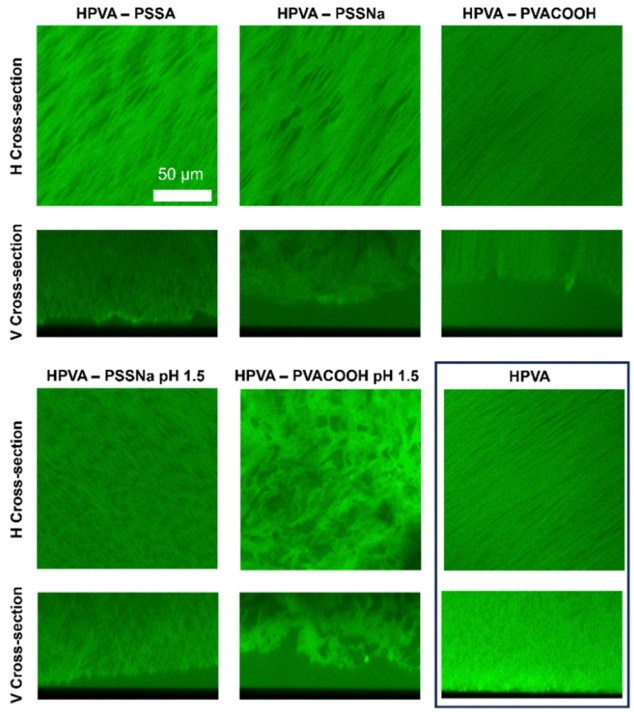

Fig. 2 CLSM images of PVA-based cryogels, containing a highly hydrolyzed PVA (H-PVA) and charged polymer additives (poly styrene sulfonic acid, PSSA, sodium poly styrene sulfonate, PSSNa, and carboxylated PVA, PVACOOH) in a 3 : 1 ratio. The horizontal and vertical cross-sections show features of the gels' porosity and morphology at the micrometer-scale, including surface roughness. H-PVA gel images are reported as a reference system.

and finally form a sponge-like structure, further control on the gel porosity may be provided by the inclusion of charged polymers in the formulation, depending on the polymer structure and the pH conditions. In addition, charged groups can promote specific interactions at the gel–substrate interface during cleaning.

In some cases, phase-separation can be triggered between PVA and a charged polymer, obtaining a charged, sponge-like structure.

Here, partially charged polymers or polyelectrolytes were mixed with a highly hydrolyzed PVA (H-PVA), in a H-PVA : polyelectrolyte = 3 : 1 ratio, to prepare cryogels.

The effects of polystyrene sulfonic acid (PSSA), sodium polystyrene sulfonate (PSSNa) and a carboxylated, partially hydrolyzed PVA (PVACOOH) on the H-PVA gel structure were observed through confocal laser scanning microscopy (CLSM) imaging. The effects of PVA cryostructuration with the same polymers under highly acidic conditions (pH 1.5) were also investigated. In this case, after the freeze-thawing process, the gels were washed in neutral demineralized water before imaging. Fig. 2 shows the horizontal (H) and vertical (V) cross-sections of the cryogels.

The presence of charges on the polyelectrolyte chains partially disrupts the ordering of the pure H-PVA structure, where pores are needle-shaped and aligned, as clearly visible in the H cross-section. PSSA and PSSNa enlarges the pore cross-section, in average. The H-PVA–PSSNa gel shows the largest pores.

Being PVACOOH only partially charged at neutral pH, the structure of H-PVA–PVACOOH cryogels remains almost the same as that of the pure H-PVA gel. V cross-sections show a variation in the surface roughness: H-PVA–PSSA is the most jagged, while H-PVA–PVACOOH shows an even surface, with pronounced pore directionality. Rough surfaces are expected to maximize the system cleaning ability for particulate matter deposited on the degraded artistic surface.

When the pH is decreased to 1.5, disruption of pore directionality occurs in the gel containing PSSNa, probably due to the increase of the ions concentration in solution. In this case, elongated pores are replaced by irregular and more compact voids. In the H-PVA–PVACOOH system, the low pH triggers a polymer–polymer phase separation: in this condition, the additive polymer is uncharged, and the interactions between the two polymers become less favored.

As both polymers have high molecular weights, the enthalpy of mixing prevails over the entropy, and demixing occurs. As a result, the final gel shows a sponge-like structure similar to those obtained when mixing H-PVA with a partially hydrolyzed PVA,[66] but with the added feature of charged functions. Gels with charged functions can exhibit enhanced interactions with charged surfaces or particulate in cleaning interventions.

As mentioned above, the capture of dirt, overpaints, or solubilized coatings by gels can be favored by tuning the interconnectivity, and thus the tortuosity of sponge-like porous networks. To this end, a model system was studied by the application of different gels to a cardboard stained with a hydrophilic dye (tartrazine) to simulate the removal of water-soluble dirt from a substrate.

In this section, to investigate the link between porosity and tortuosity and gels' transport properties, a set of three gels obtained by freeze-thawing solutions of H-PVA mixed with partially hydrolyzed PVAs (L1-3) of increasing molecular weights ("twin-chain" polymer networks, TC-PNs[66]) were studied by means of CLSM and fluorescence correlation spectroscopy (FCS). The molecular weight of the second PVA component increases following the series L1 < L2 < L3.

The effects of the molecular weight variation on the gels' morphology at the micrometer-scale was observed by CLSM as shown in Fig. 3. It is evident that the pore size increases with the molecular weight of the second PVA component. The latter acts as a porogen by phase-separation and demixing in the pre-gel PVA solutions.[66] A higher molecular weight causes a more pronounced phase separation, which reasonably produces larger pores in the final TC-PN gel. The surface roughness is expected to increase with the pores size (see vertical cross-sections, Fig. 3).

Gel cleaning performances were tested using a tartrazine-dyed cardboard. HPVA – L3 showed the highest removal ability (see Fig. 4(A) and Table 1), measured as the average of the pixels greyscale intensity in a 15 mm^2 area after conversion of the cleaned areas' images in grayscale (see Materials and methods section).

Gels' tortuosity, related to the cleaning ability, was calculated through eqn (1): D_{gel} and D_{sol} were obtained from the FCS data.

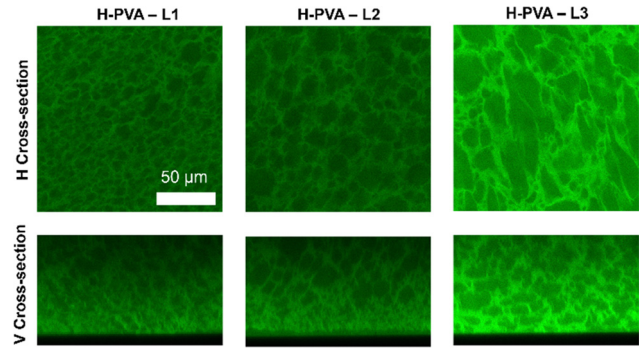

Fig. 3 CLSM images of TC-PN gels with modulated pores, containing L-PVA of increasing molecular weights: L1 < L2 < L3.

Measurements were performed on gels (loaded with the solution of a standard dye, Alexa Fluor, right after the interaction of the gels with the tartrazine-stained cardboard) and on a tartrazine-aqueous solution (at the same concentration used to stain the cardboards) containing Alexa Fluor, as well.

Namely, D_{sol} and D_{gel} represent, respectively, the diffusion coefficient of the standard dye in the tartrazine aqueous solution and in the tartrazine-loaded gel, right after the interaction with the cardboard (see Materials and methods section).

H-PVA – L1 shows the lowest apparent tortuosity. Even if the porosity changes drastically throughout the L1-3 series, the apparent tortuosity remains unaltered in the H-PVA – L2 and H-PVA – L3 gels (Fig. 4(B) and Table 1).

Overall, this suggests that the connectivity between pores is not exclusively determined by the size or shape of the phase separated domains in the pre-gel solution, but rather by the probability of their interconnection during the freezing and gelation steps.

This approach highlighted differences in the gels' transport properties over other interactions occurring at the gel–cardboard interface. The better cleaning performance of H-PVA – L3 over L2 is likely due to the different pore sizes. While the apparent tortuosity is comparable, the higher surface roughness of H-PVA – L3 is expected to increase the number of contact points with the cardboard surface, favoring homogeneous and more complete cleaning.

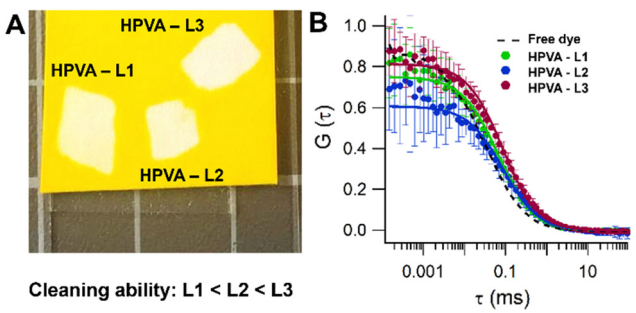

Fig. 4 The cleaning ability of TC-PN gels with modulated pores (A) can be related, to some extent, to the gels' tortuosity. (B) FCS curves and fitting, describing the diffusion of a standard dye in a tartrazine aqueous solution (free dye) and in H-PVA – L1, HPVA – L2 and HPVA – L3 gels, right after the interaction with the cardboard in (A).

Table 1 Cleaning performances of H-PVA-L1 – L3 gels: average greyscale intensity of pixels in the cleaned areas (0: black, 255: white). Diffusion coefficients (D) of the dye Alexa Fluor in a tartrazine aqueous solution (free dye) and in TC-PNs with the increasing pore size. The apparent tortuosity, τ_{app}^2, was calculated according to eqn (1)

Gel	Greyscale intensity in the cleaned areas	D (μm^2 s^{-1})	τ_{app}^2
Free dye	—	278 ± 14	—
H-PVA – L1	231 ± 2	128 ± 14	1.7
H-PVA – L2	233 ± 4	131 ± 8	2.2
H-PVA – L3	240 ± 2	168 ± 8	2.1

Ultra-adaptive, adhesive formulations for rough or vertical painted surfaces.

Another issue involves the treatment of vertical, complex surfaces. A first breakthrough was achieved for the restoration of the sculptural wall installation "Addendum" by Eva Hesse. The restoration intervention, performed at TATE Modern Gallery, London,[69] entailed the use of highly flexible gels to remove persistent soil.

Later, attempts have been made to synthetize nano-[125] and micro-structured materials with film-forming properties, which can be sprayed or brushed in nooks and folds of the artwork surface. However, optimization of the application/cleaning protocols has not yet been achieved.

In this section, new evidence will be provided about systems with improved stickiness and adaptability, namely: (i) ultra-flexible (UF) and (ii) adhesive PVA-based gels.

UF cryogels were prepared by mixing H-PVA with a high molecular weight PVP in the same proportions. Being H-PVA and PVP incompatible under these conditions,[115] large phase-separated domains, containing hydrated PVP chains, act as porogens during H-PVA cryostructuration. Two types of gels were formulated, one containing H-PVA and obtained after 1 freeze–thaw cycle (UF-HPVA), the other with a PVA characterized by a slightly lower hydrolysis degree (HD), and obtained after 6 freeze–thaw cycles (UF).

UF gels show high adaptability to complex, uneven surfaces (Fig. 5(A)).

As shown in Fig. 5(B), the US gels exhibit a lower storage modulus than TC-PNs or HPVA-PVP gels (in a 3 : 1 ratio). TC-PNs are known as highly adaptable gels for the cleaning of rough, painted surfaces.[66,67]

In this case, it was possible to tune UF gels' elasticity and improve adaptability, by varying the HD of the structural PVA. Gels prepared with a lower HD PVA (UF) needed 6 FT cycles to achieve a gel state, and showed the highest flexibility. Nonetheless, the use of H-PVA, with higher HD, allowed in obtaining gels (UF-HPVA) with exceptional flexibility after only 1 freeze–thaw cycle.

UF gels are characterized by a gel content (G%), *i.e.* the residual dry matter after washing/storage in water, that can be compared to those of H-PVA-PVP and TC-PNs gels. However, the water release is about 3 times higher: this grants the

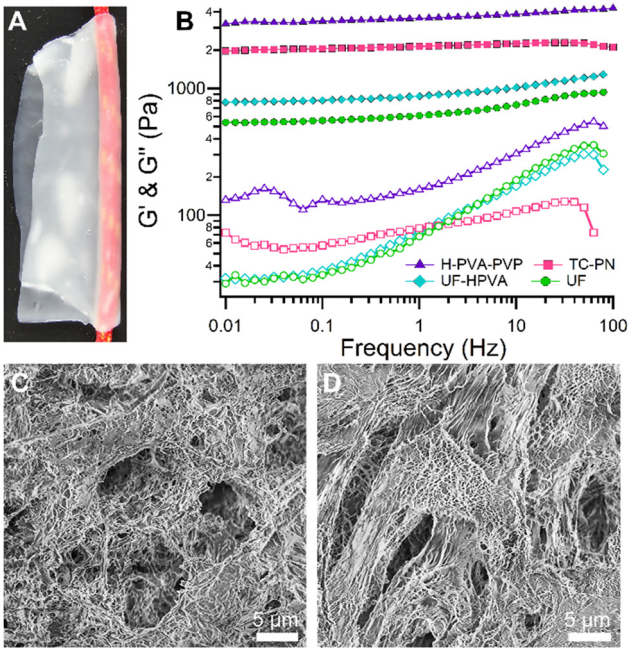

Fig. 5 (A) UF-HPVA gel adaptability to a rope, an example of rough, unconventional materials used in works of art. The gel sheet wraps homogeneously around the rope. (B) UF-HPA and UF gels' mechanical properties compared to a PVA "twin-chain" polymer network (TC-PN) and HPVA-PVP gels (3 : 1 ratio): UF gels are the less rigid; in UF gels, elasticity can be further tuned by varying PVA hydrolysis degrees. (C) and (D) SEM images of UF-HPVA (B) and UF (C) gels, showing ubiquitous pores of different size.

presence of a thicker layer of water at the gel–substrate interface during the cleaning action, which favors the removal of dirt from highly irregular surfaces (Table 2).

Moreover, UF gels are highly porous, with the pore size ranging from the tens of microns to the hundreds of nanometers (see Fig. 5(C) and (D)).

Polymers bearing charges or hydrophilic–hydrophobic groups can be used to improve gels' adhesiveness, without affecting the cohesiveness of the artwork original materials.

Gels with improved adhesiveness, to treat delicate vertical surfaces, were prepared by adding a vinyl alcohol–vinyl pyrrolidone (VA–VP) copolymer, and/or polyacrylic acid (PAA, a polyelectrolyte) to H-PVA (Fig. 6). While the VA–VP co-polymer can be used as a wetting agent and improves the gel adaptability, PAA leads to a double physical–chemical crosslinking,[126] improving gel cohesiveness: an ester bond can form between the hydroxyl group of PVA and the carboxyl group of PAA. In our case, the polymer solutions were blended at room temperature, but the process can be further enhanced at high temperatures.[126]

This type of adhesive gels easily stick to smooth surfaces, such as glazed ceramic (Fig. 6(A)).

Gels containing VA–VP are extremely soft. They deform during the adhesion to the surface (Fig. 6(B)).

On the other hand, PVA-based gels containing PAA are quite rigid and tend to detach from the same surface (Fig. 6(C)). Finally, gels containing both VA–VP and PAA are still able to closely adhere to the surface, and show better mechanical characteristic than the H-PVA–VA–VP gels (Fig. 6(D)).

Table 2 Gel contents (*G*%) and water releases of UF, PVA-PVP and TC-PN gels

Gel	*G* (%)	Water release (mg cm^{-2})
UF	47 ± 2	83 ± 7
HPVA-PVP	45 ± 1	26 ± 3
TC-PN	37 ± 1	31 ± 3

"Turning green": sustainable formulations for art remediation

Finally, one of the most compelling aspects in CH conservation involves the reduction of petroleum-based solvents and polymers.

New, eco-friendly materials are beneficial from an environmental perspective. In addition, they can replace hazardous and toxic substances detrimental for human health and harmful to the artefacts' original components.[52,71,72,76,127–131]

In this sense, biopolymer-based materials, such as natural resins and polysaccharides,[76,131–135] are gaining growing interest. Other examples include biodegradable matrices obtained from waste products of supply chains,[136,137] as well as "green" surfactants and solvents.[52,138,139]

Overall, the trend toward a re-evaluation of biopolymers traditionally used in restoration, such as agar or carboxymethyl cellulose (CMC),[130,132,140] must not be interpreted as a backtrack, but rather as a renewed awareness of the potential of natural polymers. Even though CMC is an industrial derivative of a natural biopolymer, it exhibits some relevant factors that make it a possible candidate in the formulation of new sustainable materials, including biodegradability, abundance of raw materials (it can also be obtained from agricultural waste),

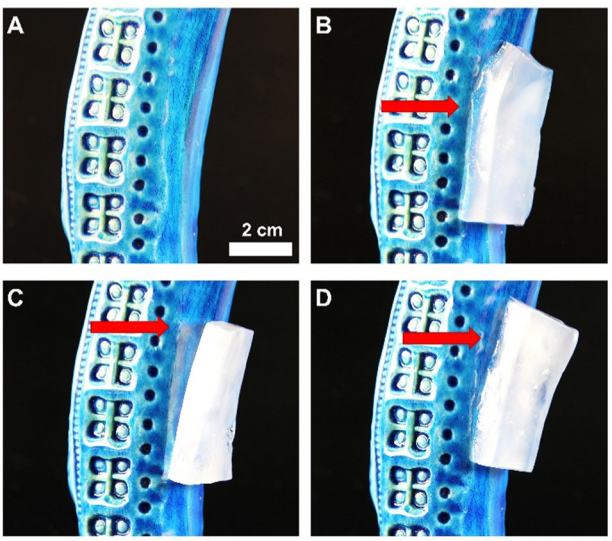

Fig. 6 Ability of sticky gels to adhere to the smooth surface of glazed ceramics (A). Gels were obtained by combining (B) H-PVA + VA–VP, (C) H-PVA + PAA, and (D) H-PVA + VA–VP + PAA. The gel containing VA–VP is extremely soft and easily sticks to the surface (B). Gels containing PAA are rigid, due to the double physical–chemical crosslinking, and tend to detach from the surface (C). When both VA–VP and PAA are added to the gel formulation, the gel easily sticks to the surface, and the gels' mechanical properties improve significantly (D).

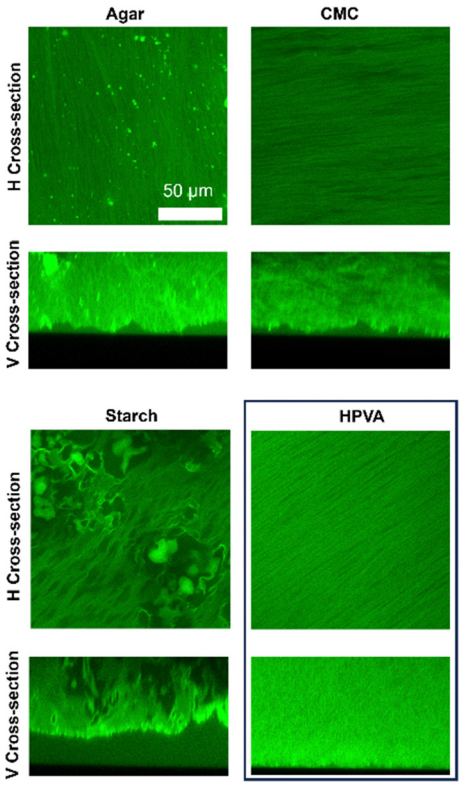

Fig. 7 CLSM images of PVA-based cryogels containing biopolymers as structural additives and/or porogens. Gels were prepared by mixing a highly hydrolyzed PVA with agar, CMC or starch, in a 4.5 : 1 ratio. The horizontal and vertical cross-sections show features of the gels' porosity and morphology at the micrometer-scale, including the surface roughness. H-PVA gel images are reported as a reference system.

biocompatibility and low toxicity, and characteristic surface properties.[141–143]

In addition, while synthetic polymers like PVA can be obtained from renewable resources, their partial replacement with biopolymers in gel formulations is an open topic in CH conservations science.

In this section, PVA-based cryogels containing H-PVA with the addition of a biopolymer are investigated. More specifically, the morphology of H-PVA-based cryogels containing agar, CMC or starch was observed through CLSM (Fig. 7).

CLSM images indicate that, in general, agar and CMC contribute to formation of gel walls, since no sponge-like structures, indicative of phase-separation in the pre-gel solution, are observed. The pores are mainly elongated and needle-shaped, such as those found in pure H-PVA gels. Nonetheless, larger pores and/or micron-sized inhomogeneities are randomly distributed throughout the matrices. Inhomogeneities result in a general increase of the gels' surface roughness (see V cross-sections in Fig. 7): micron-sized recesses and valleys characterize the surfaces of these gels. Such features favor adhesion and capture of the particulate matter during the cleaning process.

Table 3 Surface roughness of gels containing H-PVA and biopolymers. The roughness of the H-PVA gel was calculated for comparison

Gel	Roughness (%)
Agar	70 ± 18
CMC	40 ± 15
Starch	70 ± 20
HPVA	30 ± 10

Starch, on the other hand, acts both as the structuring agent and the porogen during the freeze-thawing process, as evident from the CLSM images. This is explained considering that the less soluble and crystalline amylose contributes to the formation of the gel walls, while amylopectin is expelled from the continuous phase during cryostructuration, and accumulates in micron-sized, irregularly shaped pores.[72,144]

The gels' surface roughness was calculated as the average height of the gels profiles, as shown in the vertical cross-section of Fig. 7, and considering the standard deviation. Gels with a higher roughness are those characterized by a higher value of the standard deviation. Results are listed in Table 3. Gels containing CMC are slightly rougher than H-PVA, while those containing starch and agar show the highest surface inhomogeneity.

The cleaning ability of gels with high roughness and low roughness was tested using an artificially soiled mockup mimicking the pitted surface of a modern painting. More specifically, CMC and starch-containing gels were tested and compared to the H-PVA neat gels' cleaning ability (Fig. 8).

As expected, starch showed the best cleaning performance: the higher gel roughness led to a higher soil removal from the painted surface. In the case of H-PVA and CMC gels, soil removal was much poorer.

Conclusions

Over the past few decades, nanoscale and nanostructured materials have gained fundamental relevance in the conservation of Cultural Heritage. Nanoparticles, microemulsions, gels, films/coatings and composite organic–inorganic systems are currently adopted in the consolidation, cleaning and protection of diverse artistic and historical artifacts. Recently, the focus is on the development of bio- and biomimetic systems with enhanced properties and sustainability, coping with the requirements of green chemistry. In addition to a critical overview of the main systems and applications developed in the field, this contribution provides new insights into a class of materials, the ''twin-chain''(TC) gels, which exhibit enhanced effectiveness in the removal of soil and other unwanted layers from the surface of works of art. In particular, new data were provided on the effect on cleaning capability of the gels' pore size and connectivity, or surface roughness. The inclusion of polyelectrolites and biopolymers in the gel networks based on polyvinyl alcohol (PVA) was also investigated. Tailoring the gels' morphology at the micrometer scale affected the transport properties in the gels network at the nanoscale. When higher molecular weight PVAs are used as porogens in the TC gels, the pore size and tortuosity increase, boosting the cleaning capability of the gels. In addition, modulating the porogen amount

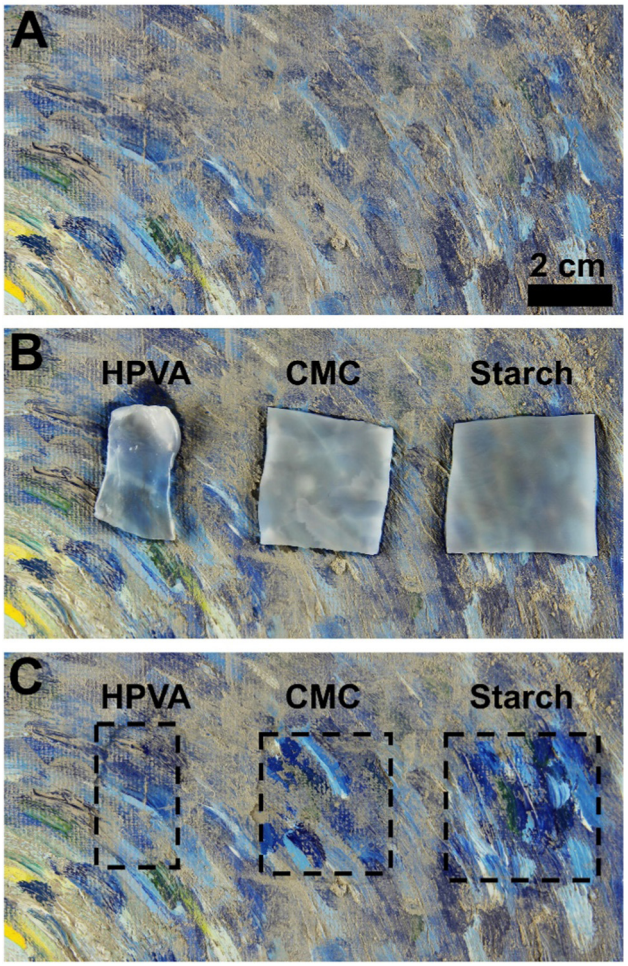

Fig. 8 Cleaning performances of gels containing biopolymers (CMC or starch) compared to the neat H-PVA gel. Cleaning tests were performed using an artificially soiled mockup, mimicking a modern painting. The higher surface roughness of the gel containing starch led to an enhanced soil removal.

or adding different polymers to PVA allows the control of the gels' surface roughness, adaptability to target surfaces, and adhesion, leading to higher cleaning efficacy and the possibility to clean rough or vertical substrates. These advancements open up new horizons in the formulation and application of nanoscale/nanostructured materials for the preservation of Cultural Heritage, with possible positive impact also in other scientific and technological fields, such as drug-delivery, detergency, food industry, cosmetics and tissue engineering.

Materials and methods

Chemicals

Highly hydrolyzed polyvinyl alcohol (H-PVA with hydrolysis degree, HD, 99% and molecular weight $M_W \sim 160$ kDa, and PVA with HD = 97–98% and molecular weight $M_W \sim 160$ kDa), polystyrene sulfonic acid (PSSA, molecular weight $M_w \sim 75$ kDa), polyvinyl pyrrolidone (PVP, molecular weight $M_n \sim 1300$ kDa), polyacrylic acid (PAA, molecular weight $M_n \sim 1200$ kDa) and carboxymethyl cellulose (CMC, molecular weight $M_W \sim 90$ kDa) for the hydrogel preparation were purchased from Sigma-Aldrich. Sodium polystyrene sulfonate (PSSNa, molecular weight $M_n \sim 77$ kDa) was purchased from Thermo-Fisher. Starch was a commercial cornstarch (Cleca, used without further purification).

The carboxylated, partially hydrolyzed PVA (PVA – COOH, Poval™ Specialty Grade 25-88 KL) and the partially hydrolyzed (HD 88%) PVAs denominated L1, L2 and L3 (Poval™ 18-88, 32-88 and 47-88, respectively) were kindly supplied by Kuraray Europe (Milan, Italy).

Selvol Ultalux SC (VA–VP copolymer) was purchased from Sekisui.

Gels were prepared in purified water (Millipore system, resistivity >18 MΩ cm). The fluorescent dyes used in CLSM or FCS measurements (rhodamine 110 chloride with purity ≥99% and Alexa Fluor 568) were purchased from Sigma-Aldrich and Thermo-Fisher Scientific, respectively. Tartrazine (dye content ≥ 85%, Sigma-Aldrich) was used in the cleaning tests and for the determination of tortuosity. Ammonium citrate tribasic (TAC, Sigma-Aldrich) was used for the removal of artificial soil from painting mock-ups.

All the chemicals were used as received, without further purification.

Gel preparation

All gels were prepared by dissolving H-PVA and any additional polymer in purified water at 95 °C, in a round-bottom flask equipped with a condenser to prevent water evaporation.

The mixtures were maintained under continuous stirring for 2 h. After complete dissolution, pre-gel solutions were cooled down to room temperature, poured into molds and frozen at −18 °C. H-PVA was mixed with PSSA, PSSNa, PVA-COOH, or L1, L2 and L3 PVAs in a 3 : 1 ratio (total polymer content: 12% w/v). UF and UF-H-PVA gels contain H-PVA or the 98% hydrolyzed PVA and PVP in a 1 : 1 ratio (total polymer content: 12% w/v). Gels with biopolymers contain a H-PVA : biopolymer ratio of 4.5 : 1 (total polymer content: 10.5% w/v). Adhesive gels were prepared by mixing a 9% w/v H-PVA solution, a 10% w/v PAA solution and a 15% w/v Ultalux (VA–VP copolymer) solution, in the following ratios: (i) H-PVA + VA–VP with H-PVA : VA–VP 9 : 1; (ii) H-PVA + PAA with H-PVA : PAA 9 : 1; (iii) H-PVA + VA–VP + PAA with H-PVA : PVA-VP (or PAA) 8.5 : 0.75.

H-PVA neat gels contain H-PVA at 9% w/v.

All gels, except UF systems, were obtained through 1 freeze–thaw cycle. UF gels were obtained after 6 freeze–thaw cycles. After thawing, gels were washed and stored in demineralized water. Water was changed daily for 7 days.

Confocal laser scanning microscopy (CLSM)

CLSM imaging was performed with a Leica TCS SP8 confocal microscope (Leica Microsystems GmbH, Wetzlar, Germany), equipped with a 63X/1.2 Zeiss objective (water immersion). Gels were soaked in a Rhodamine 110 aqueous solution before imaging. The dye was excited with a 488 nm laser line (Ar laser)

and the fluorescence was recorded using a photomultiplier tube (PMT) in the 498–540 nm range.

Fluorescence correlation spectroscopy (FCS)

FCS measurements were performed with the same CLSM used for imaging. In this case, the FCS modulus from PicoQuant (PicoQuant, Berlin, Germany) was also used. The fluorescence was recorded with a hybrid SMD detector. An aqueous solution of Alexa Fluor 568 (25 nM) was used for FCS calibration. The fitting model assumes that a three-dimensional Brownian diffusion of the fluorescent species occurs through a 3D-ellipsoidal Gaussian volume. This is considered as the only contribution to the observed decay time. FCS curves were averaged (12–15 repetitions) and analyzed according to a single-component decay:

$$G(\tau) = \frac{1}{N}\left[\left(1+\frac{\tau}{\tau_D}\right)^{-1}\left(1+\frac{\tau}{S^2\tau_D}\right)^{-1/2}\right] \quad (2)$$

where N is the average number of fluorescent molecules diffusing inside the confocal volume ($N = CV$, with $V = \pi^{3/2}w_0{}^3S$ and C the concentration), τ_D is the decay time and $S = z_0/w_0$ the ratio between the axial and the lateral dimensions of the confocal volume, determined through the calibration procedure with Alexa 568. The diffusion coefficient D can be calculated as follows:

$$\tau_D = \frac{w_0{}^2}{4D} \quad (3)$$

For the determination of gels' tortuosity, the diffusion of Alexa Fluor 568 inside TC-PN gels was measured after the gels' contact with tartrazine-dyed cardboards (10 minutes contact). For comparison, the diffusion coefficient of Alexa Fluor 568 in a concentrated tartrazine solution (2.5% w/w) was also measured.

Cleaning tests (tartrazine-dyed cardboards)

Cardboard sheets were soaked in demineralized water and then in a 2.5% w/w tartrazine aqueous solution for 1 minute. Thus, they were air-dried. TC-PN gel sheets were gently dried on Whatman® paper and placed in contact with the dyed cardboard for 10 minutes. A 10 minutes contact time is approximately the time required for the tartrazine solution, formed at the gel–cardboard interface, to diffuse within the whole gel volume (gel thickness: 2 mm; data acquired on similar gels[115]). Images of the cleaned cardboard were acquired and converted in grayscale with ImageJ, evaluating the removal by calculating the average grayscale intensity as previously reported.[115]

Effective relative diffusivity and tortuosity

The apparent tortuosity of gels was calculated as the reciprocal of the effective relative diffusivity,[119,120] and more specifically as:

$$\tau_{app}{}^2 = \frac{\tau^2}{\varepsilon} = \frac{D_{sol}}{D_{gel}} \quad (4)$$

where τ^2 is the tortuosity factor and τ is the geometrical tortuosity, while ε is the gels porosity. τ^2/ε was calculated for gels after the interaction with tartrazine-dyed cardboards, *i.e.* after the cleaning tests (10 minutes interactions). The gels apparent tortuosity factor was calculated considering the diffusion coefficients of the dye Alexa Fluor 568 in a tartrazine aqueous solution (D_{Sol}) and inside the gels (D_{Gel}), respectively. Both D_{Sol} and D_{Gel} were obtained from FCS measurements.

Rheometry

Rheology measurements were performed with a Discovery HR-3 rheometer from TA Instruments, equipped with a Peltier temperature control system. The 40 mm parallel plate geometry was used. Amplitude sweeps, to identify the linear viscoelastic range (LVE), and frequency sweeps, were performed at 25 °C. Frequency sweep curves were acquired within the LVE range, at a constant oscillation strain (0.5%), by increasing the oscillation frequency.

Scanning electron microscopy (SEM)

SEM imaging was performed using an Field Emission Gun Scanning Electron Microscope by SIGMA (FEGSEM, Carl Zeiss Microscopy GmbH, Germany), with an acceleration potential of 2 kV and a working distance of 3.5 mm. Gel samples were freeze-dried and coated with an ultra-thin layer of gold using an Auto Sputter Coater (Agar Scientific).

Gels' roughness calculation

The roughness of gels containing biopolymers was evaluated on the gels' vertical cross-sections, and more specifically by considering the average value and the relative standard deviation of each profile intensity. Briefly, the vertical cross-section images were binarized and the *XY* values of each profile were extracted through the software ImageJ. Then, *Y* values were normalized and averaged, and a standard deviation was extracted. The standard deviation can be directly related to gels' roughness, as it increases for more inhomogeneous profiles.

Preparation of alkyd painting mockups and cleaning

A mock-up mimicking a modern painting was prepared using a commercial primed canvas, oil (Windson&Newton), and alkyd colors (Ferrario). After about one year from the preparation, an artificial soil mixture in nonane[145] was applied with a brush over the paint layer. Cleaning tests were performed after one month. Gels containing H-PVA and biopolymers were soaked in a TAC aqueous solution (7% w/w) for 12 hours. TAC solutions are conservators' standard choices when the removal of particulate matter from paintings is required.[146,147] Gel sheets were gently dried with blotting papers before the application. The gel–surface contact lasted 10 minutes, in accordance with the time chosen for the tartrazine removal from cardboards.

Author contributions

RM: investigation, methodology, conceptualization, and writing – original draft; DC: conceptualization, funding acquisition, project administration, supervision, writing – original draft, and writing – review and editing; PB: conceptualization, validation, funding acquisition, methodology, project administration, supervision, and writing – review and editing.

Conflicts of interest

There are no conflicts to declare.

Acknowledgements

Dr Massimo Bricchi is gratefully acknowledged for providing PVA polymers from Kuraray. CSGI and the European Union (GREENART project, Horizon Europe research and innovation program under grant agreement no. 101060941) are gratefully acknowledged for financial support. Views and opinions expressed are however those of the author(s) only and do not necessarily reflect those of the European Union or the European Research Executive Agency (REA). Neither the European Union nor the granting authority can be held responsible for them. The publication was made by a researcher (RM) with a research contract co-funded by the European Union – PON Research and Innovation 2014–2020 in accordance with Article 24, paragraph 3a of Law no. 240 of December 30, 2010, as amended and Ministerial Decree no. 1062 of August 10, 2021.

References

1 E. Roduner, *Chem. Soc. Rev.*, 2006, **35**, 583–592.
2 L. A. Kolahalam, I. V. Kasi Viswanath, B. S. Diwakar, B. Govindh, V. Reddy and Y. L. N. Murthy, *Mater. Today: Proc.*, 2019, **18**, 2182–2190.
3 N. Baig, I. Kammakakam and W. Falath, *Mater. Adv.*, 2021, **2**, 1821–1871.
4 C. N. R. Rao and A. K. Cheetham, *J. Mater. Chem.*, 2001, **11**, 2887–2894.
5 A. Mehdi, C. Reye and R. Corriu, *Chem. Soc. Rev.*, 2011, **40**, 563–574.
6 Z. Liu, F. Kiessling and J. Gätjens, *J. Nanomater.*, 2010, **2010**, e894303.
7 A. Jawed, V. Saxena and L. M. Pandey, *J. Water Process. Eng.*, 2020, **33**, 101009.
8 P. Makvandi, S. Iftekhar, F. Pizzetti, A. Zarepour, E. N. Zare, M. Ashrafizadeh, T. Agarwal, V. V. T. Padil, R. Mohammadinejad, M. Sillanpaa, T. K. Maiti, G. Perale, A. Zarrabi and F. Rossi, *Environ. Chem. Lett.*, 2021, **19**, 583–611.
9 J.-H. Song, S.-H. Min, S.-G. Kim, Y. Cho and S.-H. Ahn, *Int. J. Jpn. Soc. Precis. Eng.*, 2022, **9**, 323–347.
10 W. Bian, Y. Wang, Z. Pan, N. Chen, X. Li, W.-L. Wong, X. Liu, Y. He, K. Zhang and Y.-J. Lu, *ACS Appl. Nano Mater.*, 2021, **4**, 11353–11385.
11 P. Baglioni, E. Carretti and D. Chelazzi, *Nat. Nanotechnol.*, 2015, **10**, 287–290.
12 M. Leona, K. Fukunaga, H. Liang, P. Baglioni, G. Festa and V. Levchenko, *Nat. Rev. Phys.*, 2021, **3**, 681–684.
13 I. Serafini and A. Ciccola, in *Nanotechnologies and Nanomaterials for Diagnostic, Conservation and Restoration of Cultural Heritage*, ed. G. Lazzara and R. Fakhrullin, Elsevier, 2019, pp.325–380.
14 P. Baglioni and D. Chelazzi, *Nanoscience for the Conservation of Works of Art*, Royal Society of Chemistry, 2013.
15 P. Baglioni, D. Chelazzi and R. Giorgi, *Nanotechnologies in the Conservation of Cultural Heritage: A compendium of materials and techniques*, Springer, Netherlands, 2015.
16 G. Lazzara, *Nanotechnologies and Nanomaterials for Diagnostic, Conservation and Restoration of Cultural Heritage*, Elsevier, Amsterdam, Netherlands, Cambridge, MA, 1st edn, 2018.
17 M. E. David, R.-M. Ion, R. M. Grigorescu, L. Iancu and E. R. Andrei, *Materials*, 2020, **13**, 2064.
18 P. Baglioni and R. Giorgi, *Soft Matter*, 2006, **2**, 293–303.
19 P. Baglioni, D. Chelazzi, R. Giorgi and G. Poggi, *Langmuir*, 2013, **29**, 5110–5122.
20 P. Baglioni and D. Chelazzi, *Chem. – Eur. J.*, 2021, **27**, 10798–10806.
21 M. Baglioni, G. Poggi, D. Chelazzi and P. Baglioni, *Molecules*, 2021, **26**, 3967.
22 C. Saiz-Jimenez, *Appl. Sci.*, 2023, **13**, 1824.
23 G. Piñar and K. Sterflinger, *Microb. Biotechnol.*, 2021, **14**, 806–809.
24 M. Lhermitte, B. Perrin and L. Melbouci, *Creating Growth: Measuring Cultural and Creative Markets in the EU*, 2014, pp. 5–97.
25 S. Prati, G. Sciutto, I. Bonacini and R. Mazzeo, in *Analytical Chemistry for Cultural Heritage*, ed. R. Mazzeo, Springer International Publishing, Cham, 2017, pp.129–160.
26 B. Giovanni Brunetti, *Acc. Chem. Res.*, 2010, **43**, 693–694.
27 A. Sgamellotti, B. G. Brunetti and C. Miliani, *Science and Art: The Painted Surface*, Royal Society of Chemistry, 2014.
28 J. Jehlička and A. Culka, *Anal. Chim. Acta*, 2022, **1209**, 339027.
29 G. Bitossi, R. Giorgi, M. Mauro, B. Salvadori and L. Dei, *Appl. Spectrosc. Rev.*, 2005, **40**, 187–228.
30 S. Svanberg, *Appl. Phys. B*, 2008, **92**, 351–358.
31 E. Martinho and A. Dionísio, *J. Geophys. Eng.*, 2014, **11**, 053001.
32 A. Romani, C. Clementi, C. Miliani and G. Favaro, *Acc. Chem. Res.*, 2010, **43**, 837–846.
33 A. Moropoulou, N. P. Avdelidis, M. Karoglou, E. T. Delegou, E. Alexakis and V. Keramidas, *Appl. Sci.*, 2018, **8**, 284.
34 A. K. Adya and E. Canetta, in *Animal Biotechnology*, ed. A. S. Verma and A. Singh, Academic Press, San Diego, 2014, pp.247–263.
35 P. Barman, S. Sharma and A. Saini, in *Photophysics and Nanophysics in Therapeutics*, ed. N. M. Mahajan, A. Saini, N. A. Raut and S. J. Dhoble, Elsevier, 2022, pp.379–418.
36 M. Filella, in *Comprehensive Sampling and Sample Preparation*, ed. J. Pawliszyn, Academic Press, Oxford, 2012, pp.109–124.
37 S. Mitragotri, D. G. Anderson, X. Chen, E. K. Chow, D. Ho, A. V. Kabanov, J. M. Karp, K. Kataoka, C. A. Mirkin, S. H. Petrosko, J. Shi, M. M. Stevens, S. Sun, S. Teoh, S. S. Venkatraman, Y. Xia, S. Wang, Z. Gu and C. Xu, *ACS Nano*, 2015, **9**, 6644–6654.
38 E. Ryabchikova, *Nanomaterials*, 2021, **11**, 118.
39 L. Bertrand, C. Gervais, A. Masic and L. Robbiola, *Angew. Chem., Int. Ed.*, 2018, **57**, 7288–7295.

40 J. Spadavecchia, E. Apchain, M. Albéric, E. Fontan and I. Reiche, *Angew. Chem., Int. Ed.*, 2014, **53**, 8363–8366.
41 P. Walter, E. Welcomme, P. Hallégot, N. J. Zaluzec, C. Deeb, J. Castaing, P. Veyssière, R. Bréniaux, J.-L. Lévêque and G. Tsoucaris, *Nano Lett.*, 2006, **6**, 2215–2219.
42 F. Ridi, E. Fratini and P. Baglioni, *J. Colloid Interface Sci.*, 2011, **357**, 255–264.
43 P. Glavič, Z. N. Pintarič and M. Bogataj, *Processes*, 2021, **9**, 148.
44 S. Filipović, N. Lior and M. Radovanović, *Renewable Sustainable Energy Rev.*, 2022, **168**, 112759.
45 M. J. Mulvihill, E. S. Beach, J. B. Zimmerman and P. T. Anastas, *Annu. Rev. Environ. Resour.*, 2011, **36**, 271–293.
46 J. B. Zimmerman, P. T. Anastas, H. C. Erythropel and W. Leitner, *Science*, 2020, **367**, 397–400.
47 K. L. Mulholland, R. W. Sylvester and J. A. Dyer, *Environ. Prog.*, 2000, **19**, 260–268.
48 D. Prat, A. Wells, J. Hayler, H. Sneddon, C. Robert McElroy, S. Abou-Shehada and P. J. Dunn, *Green Chem.*, 2016, **18**, 288–296.
49 D. Morelli Venturi, F. Campana, F. Marmottini, F. Costantino and L. Vaccaro, *ACS Sustainable Chem. Eng.*, 2020, **8**, 17154–17164.
50 E. Semenzin, E. Giubilato, E. Badetti, M. Picone, A. Volpi Ghirardini, D. Hristozov, A. Brunelli and A. Marcomini, *Environ. Sci. Pollut. Res.*, 2019, **26**, 26146–26158.
51 M. Menegaldo, A. Livieri, P. Isigonis, L. Pizzol, A. Tyrolt, A. Zabeo, E. Semenzin and A. Marcomini, *Clean. Environ. Syst.*, 2023, **9**, 100124.
52 A. Casini, D. Chelazzi and P. Baglioni, *Sci. China: Technol. Sci.*, 2023, **66**, 2162–2182.
53 *Gels and Other Soft Amorphous Solids*, ed. F. Horkay, J. F. Douglas and E. D. Gado, American Chemical Society, Washington, DC, 2019.
54 D. Chelazzi, R. Giorgi and P. Baglioni, *Angew. Chem., Int. Ed.*, 2018, **57**, 7296–7303.
55 L. V. Angelova, B. Ormsby, J. H. Townsend and R. Wolbers, *Gels in the Conservation of Art*, Archetype Pubns, London, 2017.
56 D. Chelazzi, R. Bordes, R. Giorgi, K. Holmberg and P. Baglioni, *Curr. Opin. Colloid Interface Sci.*, 2020, **45**, 108–123.
57 M. Baglioni, C. Montis, D. Chelazzi, R. Giorgi, D. Berti and P. Baglioni, *Angew. Chem., Int. Ed.*, 2018, **130**, 7477–7481.
58 M. Baglioni, F. H. Sekine, T. Ogura, S.-H. Chen and P. Baglioni, *J. Colloid Interface Sci.*, 2022, **606**, 124–134.
59 M. Baglioni, T. Guaragnone, R. Mastrangelo, F. H. Sekine, T. Ogura and P. Baglioni, *ACS Appl. Mater. Interfaces*, 2020, **12**, 26704–26716.
60 M. Baglioni, M. Alterini, D. Chelazzi, R. Giorgi and P. Baglioni, *Front. Mater*, 2019, **6**, 311.
61 B. Ormsby, M. Keefe, A. Phenix, E. von Aderkas, T. Learner, C. Tucker and C. Kozak, *J. Am. Inst. Conserv.*, 2016, **55**, 12–31.
62 V. Chauhan, K. Holmberg and R. Bordes, *J. Colloid Interface Sci.*, 2018, **531**, 189–193.
63 N. Bonelli, C. Montis, A. Mirabile, D. Berti and P. Baglioni, *Proc. Natl. Acad. Sci. U. S. A.*, 2018, **115**, 5932–5937.
64 M. Baglioni, J. A. L. Domingues, E. Carretti, E. Fratini, D. Chelazzi, R. Giorgi and P. Baglioni, *ACS Appl. Mater. Interfaces*, 2018, **10**, 19162–19172.
65 T. Guaragnone, M. Rossi, D. Chelazzi, R. Mastrangelo, M. Severi, E. Fratini and P. Baglioni, *ACS Appl. Mater. Interfaces*, 2022, **14**, 7471–7485.
66 R. Mastrangelo, D. Chelazzi, G. Poggi, E. Fratini, L. P. Buemi, M. L. Petruzzellis and P. Baglioni, *Proc. Natl. Acad. Sci. U. S. A.*, 2020, **117**, 7011–7020.
67 L. Pensabene Buemi, M. L. Petruzzellis, D. Chelazzi, M. Baglioni, R. Mastrangelo, R. Giorgi and P. Baglioni, *Heritage Sci.*, 2020, **8**, 77.
68 A. Bartoletti, R. Barker, D. Chelazzi, N. Bonelli, P. Baglioni, J. Lee, L. V. Angelova and B. Ormsby, *Heritage Sci.*, 2020, **8**, 9.
69 A. Bartoletti, T. Maor, D. Chelazzi, N. Bonelli, P. Baglioni, L. V. Angelova and B. A. Ormsby, *Heritage Sci.*, 2020, **8**, 35.
70 M. Baglioni, R. Mastrangelo, P. Tempesti, T. Ogura and P. Baglioni, *Colloids Surf., A*, 2023, **660**, 130857.
71 G. Poggi, H. D. Santan, J. Smets, D. Chelazzi, D. Noferini, M. L. Petruzzellis, L. Pensabene Buemi, E. Fratini and P. Baglioni, *J. Colloid Interface Sci.*, 2023, **638**, 363–374.
72 V. Rosciardi, D. Chelazzi and P. Baglioni, *J. Colloid Interface Sci.*, 2022, **613**, 697–708.
73 J. Yiming, G. Sciutto, S. Prati, E. Catelli, M. Galeotti, S. Porcinai, L. Mazzocchetti, C. Samorì, P. Galletti, L. Giorgini, E. Tagliavini and R. Mazzeo, *Heritage Sci.*, 2019, **7**, 34.
74 Y. Çakmak, E. Çakmakçi, N. K. Apohan and R. Karadag, *J. Cult. Herit.*, 2022, **55**, 391–398.
75 G. Cavallaro, S. Milioto, L. Nigamatzyanova, F. Akhatova, R. Fakhrullin and G. Lazzara, *ACS Appl. Nano Mater.*, 2019, **2**, 3169–3176.
76 A. Passaretti, L. Cuvillier, G. Sciutto, E. Guilminot and E. Joseph, *Appl. Sci.*, 2021, **11**, 3405.
77 S. Prati, F. Volpi, R. Fontana, P. Galletti, L. Giorgini, R. Mazzeo, L. Mazzocchetti, C. Samorì, G. Sciutto and E. Tagliavini, *Pure Appl. Chem.*, 2018, **90**, 239–251.
78 D. Chelazzi, G. Poggi, Y. Jaidar, N. Toccafondi, R. Giorgi and P. Baglioni, *J. Colloid Interface Sci.*, 2013, **392**, 42–49.
79 C. Rodriguez-Navarro and E. Ruiz-Agudo, *Pure Appl. Chem.*, 2018, **90**, 523–550.
80 C. Rodriguez-Navarro, A. Suzuki and E. Ruiz-Agudo, *Langmuir*, 2013, **29**, 11457–11470.
81 R. Camerini, G. Poggi, D. Chelazzi, F. Ridi, R. Giorgi and P. Baglioni, *J. Colloid Interface Sci.*, 2019, **547**, 370–381.
82 C. Rodriguez-Navarro, I. Vettori and E. Ruiz-Agudo, *Langmuir*, 2016, **32**, 5183–5194.
83 R. Camerini, D. Chelazzi, R. Giorgi and P. Baglioni, *J. Colloid Interface Sci.*, 2019, **539**, 504–515.
84 R. Giorgi, D. Chelazzi and P. Baglioni, *Appl. Phys. A: Mater. Sci. Process.*, 2006, **83**, 567–571.
85 R. Giorgi, D. Chelazzi, E. Fratini, S. Langer, A. Niklasson, M. Rådemar, J.-E. Svensson and P. Baglioni, *J. Cult. Herit.*, 2009, **10**, 206–213.

86 M. Baglioni, A. Bartoletti, L. Bozec, D. Chelazzi, R. Giorgi, M. Odlyha, D. Pianorsi, G. Poggi and P. Baglioni, *Appl. Phys. A: Mater. Sci. Process.*, 2016, **122**, 114.
87 D. Chelazzi, R. Giorgi and P. Baglioni, *Macromol. Symp.*, 2006, **238**, 30–36.
88 E. J. Schofield, R. Sarangi, A. Mehta, A. M. Jones, A. Smith, J. F. W. Mosselmans and A. V. Chadwick, *J. Cult. Herit.*, 2016, **18**, 306–312.
89 M. José Alves Oliveira, L. Otubo, A. Pires, R. Fernando Brambilla, A. Cristina Carvalho, P. S. Santos, A. Oliveira Neto and P. Vasquez, *Radiat. Phys. Chem.*, 2022, **199**, 110345.
90 J. Becerra, M. Mateo, P. Ortiz, G. Nicolás and A. P. Zaderenko, *J. Cult. Herit.*, 2019, **38**, 126–135.
91 M. S. Waghmode, A. B. Gunjal, J. A. Mulla, N. N. Patil and N. N. Nawani, *SN Appl. Sci.*, 2019, **1**, 310.
92 M. F. La Russa, S. A. Ruffolo, N. Rovella, C. M. Belfiore, A. M. Palermo, M. T. Guzzi and G. M. Crisci, *Prog. Org. Coat.*, 2012, **74**, 186–191.
93 A. Carrapiço, M. R. Martins, A. T. Caldeira, J. Mirão and L. Dias, *Microorganisms*, 2023, **11**, 378.
94 A. Zuliani, D. Chelazzi, R. Mastrangelo, R. Giorgi and P. Baglioni, *J. Colloid Interface Sci.*, 2023, **632**, 74–86.
95 A. Zuliani, D. Bandelli, D. Chelazzi, R. Giorgi and P. Baglioni, *J. Colloid Interface Sci.*, 2022, **614**, 451–459.
96 M. Salzano de Luna, G. G. Buonocore, C. Giuliani, E. Messina, G. Di Carlo, M. Lavorgna, L. Ambrosio and G. M. Ingo, *Angew. Chem., Int. Ed.*, 2018, **57**, 7380–7384.
97 A. Presentato, F. Armetta, A. Spinella, D. F. Chillura Martino, R. Alduina and M. L. Saladino, *Front. Chem*, 2020, **8**, 699.
98 G. Cavallaro, S. Milioto and G. Lazzara, *Langmuir*, 2020, **36**, 3677–3689.
99 G. Lo Dico, F. Semilia, S. Milioto, F. Parisi, G. Cavallaro, G. Inguì, M. Makaremi, P. Pasbakhsh and G. Lazzara, *Appl. Sci.*, 2018, **8**, 1455.
100 C. H. M. Camargos, G. Poggi, D. Chelazzi, P. Baglioni and C. A. Rezende, *ACS Appl. Nano Mater.*, 2022, **5**, 13245–13259.
101 C. Cianci, D. Chelazzi, G. Poggi, F. Modi, R. Giorgi and M. Laurati, *Colloids Surf., A*, 2022, **634**, 127944.
102 A. Casini, D. Chelazzi and R. Giorgi, *ACS Appl. Mater. Interfaces*, 2021, **13**, 37924–37936.
103 J. Zhao, M. Sun, Z. Pan, B. Liu, M. Ostadhassan and Q. Hu, *Adv. Geo-Energy Res.*, 2022, **6**, 54–68.
104 C. Schröfl, K. A. Erk, W. Siriwatwechakul, M. Wyrzykowski and D. Snoeck, *Cem. Concr. Res.*, 2022, **151**, 106648.
105 M. Sauerwein and H. Steeb, *Int. J. Eng. Sci.*, 2020, **155**, 103353.
106 L. Ma, X. Luo, N. Cai, Y. Xue, S. Zhu, Z. Fu and F. Yu, *Appl. Surf. Sci.*, 2014, **305**, 186–193.
107 J. H. Petropoulos, in *Polymer Membranes*, ed. M. Gordon, Springer, Berlin, Heidelberg, 1985, pp.93–142.
108 S. A. Piletsky, T. L. Panasyuk, E. V. Piletskaya, I. A. Nicholls and M. Ulbricht, *J. Membr. Sci.*, 1999, **157**, 263–278.
109 H. K. Lonsdale, U. Merten and R. L. Riley, *J. Appl. Polym. Sci.*, 1965, **9**, 1341–1362.
110 A. Szymczyk and P. Fievet, *J. Membr. Sci.*, 2005, **252**, 77–88.
111 M. Matyka, A. Khalili and Z. Koza, *Phys. Rev. E: Stat., Nonlinear, Soft Matter Phys.*, 2008, **78**, 026306.
112 J. van Brakel and P. M. Heertjes, *Int. J. Heat Mass Transfer*, 1974, **17**, 1093–1103.
113 F. V. Luna, A. K. Maurya, J. M. de Souza e Silva, G. Dittrich, T. Paul, D. Enke, P. Huber, R. Wehrspohn and M. Steinhart, *J. Phys. Chem. C*, 2022, **126**, 12765–12779.
114 T. Miao, A. Chen, Y. Xu, S. Cheng and B. Yu, *Fractals*, 2019, **27**, 1950121.
115 R. Mastrangelo, C. Resta, E. Carretti, E. Fratini and P. Baglioni, *ACS Appl. Mater. Interfaces*, 2023, **15**, 46428–46439.
116 J. Hurler, A. Engesland, B. Poorahmary Kermany and N. Škalko-Basnet, *J. Appl. Polym. Sci.*, 2012, **125**, 180–188.
117 M. Huang, J. F. Kennedy, B. Li, X. Xu and B. J. Xie, *Carbohydr. Polym.*, 2007, **69**, 411–418.
118 M. Lombardo, G. Carbone, G. Lombardo, M. P. De Santo and R. Barberi, *J. Cataract Refractive Surg.*, 2009, **35**, 1266.
119 N. Koone, Y. Shao and T. W. Zerda, *J. Phys. Chem.*, 1995, **99**, 16976–16981.
120 B. Tjaden, D. J. L. Brett and P. R. Shearing, *Int. Mater. Rev.*, 2018, **63**, 47–67.
121 F. Dehli, L. Rebers, C. Stubenrauch and A. Southan, *Biomacromolecules*, 2019, **20**, 2666–2674.
122 K. Flégeau, R. Pace, H. Gautier, G. Rethore, J. Guicheux, C. Le Visage and P. Weiss, *Adv. Colloid Interface Sci.*, 2017, **247**, 589–609.
123 Z. Zhang, H. Tan, Y. Zhao, Q. Wang and H. Wang, *J. Colloid Interface Sci.*, 2019, **553**, 40–49.
124 J. A. L. Domingues, N. Bonelli, R. Giorgi, E. Fratini, F. Gorel and P. Baglioni, *Langmuir*, 2013, **29**, 2746–2755.
125 S. Vicini, M. Castellano, M. Mauri and E. Marsano, *Carbohydr. Polym.*, 2015, **134**, 767–774.
126 K. Kumeta, I. Nagashima, S. Matsui and K. Mizoguchi, *J. Appl. Polym. Sci.*, 2003, **90**, 2420–2427.
127 Y. Jia, G. Sciutto, R. Mazzeo, C. Samorì, M. L. Focarete, S. Prati and C. Gualandi, *ACS Appl. Mater. Interfaces*, 2020, **12**, 39620–39629.
128 B. Di Napoli, S. Franco, L. Severini, M. Tumiati, E. Buratti, M. Titubante, V. Nigro, N. Gnan, L. Micheli, B. Ruzicka, C. Mazzuca, R. Angelini, M. Missori and E. Zaccarelli, *ACS Appl. Polym. Mater.*, 2020, **2**, 2791–2801.
129 M. Di Vito, M. G. Bellardi, P. Colaizzi, D. Ruggiero, C. Mazzuca, L. Micheli, S. Sotgiu, S. Iannuccelli, M. Michelozzi, F. Mondello, P. Mattarelli and M. C. Sclocchi, *Stud. Conserv.*, 2018, **63**, 13–23.
130 A. Sansonetti, M. Bertasa, C. Canevali, A. Rabbolini, M. Anzani and D. Scalarone, *J. Cult. Herit.*, 2020, **44**, 285–296.
131 C. Mazzuca, L. Micheli, R. Lettieri, E. Cervelli, T. Coviello, C. Cencetti, S. Sotgiu, S. Iannuccelli, G. Palleschi and A. Palleschi, *Microchem. J.*, 2016, **126**, 359–367.
132 G. De Filpo, A. M. Palermo, R. Tolmino, P. Formoso and F. P. Nicoletta, *Cellulose*, 2016, **23**, 3265–3279.
133 G. Infurna, G. Cavallaro, G. Lazzara, S. Milioto and N. T. Dintcheva, *Molecules*, 2021, **26**, 3468.
134 A. Giordano, M. R. Caruso and G. Lazzara, *Heritage Sci.*, 2022, **10**, 123.
135 C. Lee, F. Volpi, G. Fiocco, M. L. Weththimuni, M. Licchelli and M. Malagodi, *Materials*, 2022, **15**, 1100.

136 M. Hernández-Escampa, F. Rodríguez-Acuña, F. Millán-Cruz, P. Rodríguez-Rojas, M. Hernández-Gallegos, A. Covelo, C. Menchaca-Campos and J. Uruchurtu, *Int. J. Polym. Sci.*, 2013, **2013**, e751056.
137 M. de Silva and J. Henderson, *J. Inst. Conserv.*, 2011, **34**, 5–15.
138 S. De, S. Malik, A. Ghosh, R. Saha and B. Saha, *RSC Adv.*, 2015, **5**, 65757–65767.
139 C. J. Clarke, W.-C. Tu, O. Levers, A. Bröhl and J. P. Hallett, *Chem. Rev.*, 2018, **118**, 747–800.
140 K. Kolman, O. Nechyporchuk, M. Persson, K. Holmberg and R. Bordes, *Colloids Surf., A*, 2017, **532**, 420–427.
141 M. S. Rahman, M. S. Hasan, A. S. Nitai, S. Nam, A. K. Karmakar, M. S. Ahsan, M. J. A. Shiddiky and M. B. Ahmed, *Polymers*, 2021, **13**, 1345.
142 J. S. Yaradoddi, N. R. Banapurmath, S. V. Ganachari, M. E. M. Soudagar, N. M. Mubarak, S. Hallad, S. Hugar and H. Fayaz, *Sci. Rep.*, 2020, **10**, 21960.
143 V. Miljković, I. Gajić and L. Nikolić, *Polymers*, 2021, **13**, 4115.
144 V. Rosciardi and P. Baglioni, *J. Colloid Interface Sci.*, 2023, **630**, 415–425.
145 B. Ormsby, A. Soldano, M. H. Keefe, A. Phenix and T. Learner, An Empirical Evaluation of a Range of Cleaning Agents for Removing Dirt from Artists' Acrylic Emulsion Paints, 2010, 23, 77–87.
146 P. Cremonesi, *L'ambiente acquoso per la pulitura di opere policrome*, Il Prato, 2011.
147 R. Wolbers, *Un approccio acquoso alla pulitura dei dipinti*, Il Prato, 2004.